

Accretion onto Stars with Octupole Magnetic Fields: Matter Flow, Hot Spots and Phase Shifts

Min Long^a, Marina M. Romanova^b, Frederick K. Lamb^{c,d}

^aCenter for Theoretical Astrophysics, Department of Physics, University of Illinois at Urbana-Champaign, 1110 W Green St., Urbana, IL 61801, email: longm@illinois.edu

^bDepartment of Astronomy, Cornell University, Ithaca, NY 14853, email: romanova@astro.cornell.edu

^cCenter for Theoretical Astrophysics, Department of Physics, University of Illinois at Urbana-Champaign, 1110 W Green St., Urbana, IL 61801, email: fkl@illinois.edu

^dAlso Department of Astronomy

Abstract

Recent measurements of the surface magnetic fields of classical T Tauri stars (CTTSs) and magnetic cataclysmic variables show that their magnetic fields have a complex structure. Investigation of accretion onto such stars requires global three-dimensional (3D) magnetohydrodynamic (MHD) simulations, where the complexity of simulations strongly increases with each higher-order multipole. Previously, we were able to model disc accretion onto stars with magnetic fields described by a superposition of dipole and quadrupole moments. However, in some stars, like CTTS V2129 Oph and BP Tau, the octupolar component is significant and it was necessary to include the next octupolar component. Here, we show results of global 3D MHD simulations of accretion onto stars with superposition of the dipole and octupole fields, where we vary the ratio between components. Simulations show that if octupolar field strongly dominates at the disc-magnetosphere boundary, then matter flows into the ring-like octupolar poles, forming ring-shape spots at the surface of the star above and below equator. The light-curves are complex and may have two peaks per period. In case where the dipole field dominates, matter accretes in two ordered funnel streams towards poles, however the polar spots are meridionally-elongated due to the action of the octupolar component. In the case when the fields are of similar strengths, both, polar and belt-like spots are present. In many cases the light-curves show the evidence of complex fields, excluding the cases of small inclinations angles, where sinusoidal light-curve is observed and ‘hides’ the information about the field complexity.

We also propose new mechanisms of phase shift in stars with complex magnetic fields. We suggest that the phase shifts can be connected with: (1) temporal variation of the star’s intrinsic magnetic field and subsequent redistribution of main magnetic poles; (2) variation of the accretion rate, which causes the disc to interact with the magnetic fields associated with different magnetic moments. We use our model to demonstrate these phase shift mechanisms, and we discuss possible applications of these mechanisms to accreting millisecond pulsars and young stars.

Keywords:

accretion, accretion discs, magnetic fields, MHD

1. Introduction

Different types of stars may have dynamically important magnetic fields. These are young classical T Tauri stars (CTTSs) (Basri, Marcy & Valenti 1992; Johns-Krull 2007), magnetic white dwarfs in some cataclysmic variables (e.g., Warner 1995; Euchner et al. 2005), and various types of neutron stars (e.g., Makishima et al. 1999, van der Klis 2000; Ghosh 2007). In most stars the structure of the field is unknown.

Measurements of the surface magnetic fields of

CTTSs using different techniques indicate that they have a complex structure (Johns-Krull, Valenti & Korosko 1999; Johns-Krull 2007). Measurements of the magnetic fields of nearby low-mass stars using the Zeeman-Doppler technique show that their fields are often complex (e.g., Donati and Collier Cameron 1997, Donati et al. 1999; Jardine et al. 2002). The observed surface field is often approximated with a set of multipoles whose magnetic moments have different misalignment angles relative to the rotational axis (i.e., differ-

ent tilts) and different phases in the longitudinal direction (e.g., Jardine et al. 2002). Recent observations of two CTTSs have shown that in one star (V2129 Oph) the surface magnetic field can be approximated with the superposition of a slightly (but differently) tilted octupole, which dominates, and a dipole, where the magnetic moments are oriented at different phases (Donati et al. 2007, 2011). In the other star, BP Tau, the magnetic field can be approximated with slightly (but differently) tilted dipole and octupole moments of equal strengths, where the magnetic moments are in anti-phase (Donati et al. 2008). Other multipoles contain much less magnetic energy. An example of these young stars shows that such a distribution might be common for some other magnetized stars.

Recently, the magnetic field structure of young stars with complex fields has been studied analytically. It was found that the fraction of the flux through the stellar surface in open field lines is smaller in stars with complex fields than in those with purely dipolar fields (Gregory et al. 2008) and a superposition of multipole fields yields smaller accretion hot spots (Mohanty & Shu 2008). The potential approximation is usually used to extrapolate the surface magnetic field to larger distances. That is, it is suggested that the field outside of the star is not disturbed by the surrounding plasma (e.g., Gregory et al. 2010). Gregory et al. (2006) calculated possible paths of gas flow around stars with magnetic fields constructed from measurements using the potential approximation. Recently, we were able to compute the flow of gas around V2129 Oph and BP Tau in global 3D MHD simulations in which the magnetic field is not assumed to be a potential field but is instead calculated as part of the simulation (Romanova et al. 2011a; Long et al. 2011).

Zeeman tomography of magnetic white dwarfs has shown that they also may have complex magnetic fields (Euchner et al. 2002). In some, such as HE 1045–0908, the magnetic field associated with the star’s quadrupole moment dominates whereas the fields associated with its dipole and octupole moments are much weaker (Euchner et al. 2005). In others, representations of the field require inclusion of tilted dipole, quadrupole, octupole, and other multipoles up to $n = 4$ or $n = 5$ (Euchner et al. 2006; Beuermann et al. 2007). These results are in accord with earlier indications of field complexity, such as asymmetric distribution of spots on the stellar surface (Meggitt & Wickramasinghe 1989; Piirola et al. 1987; see Wickramasinghe & Ferrario 2000 for a review).

Many neutron stars also have dynamically important magnetic fields. X-ray observations of the cyclotron line helped to reveal the value of the field in some neutron

stars (e.g., Makishima et al. 1999; Coburn et al. 2002 and references therein; see also Bignami et al. 2003). The magnetic fields of newly formed neutron stars may be enhanced by a dynamo mechanism (e.g., Thompson & Duncan 1993) and may have a complex structure. There is evidence that at least some accretion-powered X-ray pulsars have complex magnetic field structures (Elsner & Lamb 1976; Burderi et al. 2000; Nishimura 2005). Accreting millisecond X-ray pulsars have relatively weak magnetic fields (e.g. Psaltis & Chakrabarty 1999; van der Klis 2000). They often have almost sinusoidal light curves, or the light-curve can strongly depart from a sinusoid during the outburst and may have two peaks per period (see, e.g., Hartman et al. 2008; Poutanen, Ibragimov & Annala 2009; Ibragimov & Poutanen 2009). A sinusoidal light-curve is consistent with a dipole magnetic field with a small tilt to the spin axis. However, in stars with more complex fields, the light-curve can be also sinusoidal or almost sinusoidal, in particular at small inclination angles (e.g., Long et al. 2007, 2008; see this paper). Also, the field may be a dipole at large distances, but have more complex structure at small distances. In some theories, it is suggested that the field of millisecond pulsars could represent a strongly off-center dipole field (e.g., Ruderman 1991; Chen & Ruderman 1993), which gives us a hint that the field may be more complex than a typical dipole field.

An unusual phenomenon — rapid, relatively large shifts in the phase of the light curve — have been observed in many millisecond pulsars (e.g., Morgan et al. 2003; Markwardt 2004; Burderi et al. 2006; Hartman et al. 2008, 2009). There may be different reasons for the phase shifts. In one model, the phase shifts are connected with the motion of accretion spots on the surface of the star (e.g., Lamb et al. 2009a,b; Patruno et al. 2010). Such spot motion has been observed in global 3D simulations of disc-magnetosphere interactions (Romanova et al. 2003, 2004; Bachetti et al. 2010). In another model, it is suggested that the timing noise can be connected with variation of the pulse shapes (e.g., Poutanen et al. 2009). This problem has not been solved yet.

In this paper, we propose and investigate different types of phase shifts that can be connected with the *complexity* of stellar magnetic fields. In one mechanism, we take into account that the magnetic field of the star may vary in time, and hence the position of hot spots will vary as well; this will be observed as phase-shift of pulses. The magnetic field of young, low-mass stars may vary rapidly due to the dynamo mechanism. Spectropolarimetric observations of young CTTS stars, show that in some stars, the magnetic field can vary as

fast as one week (Donati et al. 2010; see also Smirnov et al. 2004). This mechanism is evidently important in young stars, where the magnetic field can vary rapidly; the magnetic field of compact stars varies only slowly (e.g., Ruderman 2005). It is possible, however, that the field can be varied or partially buried during periods of enhanced accretion, as we discuss later in this paper (see Sec. 5).

Another type of phase-shift can be connected with variation of the accretion rate, and it operates even in cases when the magnetic field is fixed. Namely, if the accretion rate varies, then the accretion disk interacts with different multipoles: at low accretion rates it will interact with the dipole component, which dominates at large distances; at higher accretion rates, the disc will come closer to the star and it will interact with the higher-order multipole of the complex field. The magnetic axes of multipoles can have different tilts and phases relative to one another, and hence the set of hot spots and the light-curves will be different at different accretion rates. We can expect variation in both the phases and the shape of the light-curves. We use our present stellar model with a superposition of the dipole and octupole fields to demonstrate both of the above models of phase-shifts.

3D simulations of accretion onto stars with multipolar fields are very challenging due to the steep gradients of the magnetic field. The complexity strongly increases with adding higher order multipoles. For example, in the case of the dipole field, the magnetic energy terms are on the order of $B_1^2 \sim 1/r^6$. The code should resolve the gradients of this value in the vicinity of the star. In the case of a quadrupole field, we deal with terms on the order of $B_1^2 \sim 1/r^8$, and in the case of octupolar field with terms $\sim 1/r^{10}$.

In our earlier studies, we were able to perform global 3D MHD simulations of accretion onto stars with a dipole magnetic field (Koldoba et al. 2002; Romanova et al. 2003, 2004; Kulkarni & Romanova 2005) and stars with a combination of dipole and quadrupole fields in the cases when they are aligned (Long, et al. 2007) or misaligned (Long, et al. 2008).

In this paper, we investigate accretion onto stars with an *octupole* field component. Our methods allow us to investigate the general case of a magnetic field produced by superposition of dipole, quadrupole, and octupole fields oriented in different directions. However, even the simpler case of a magnetic field produced by superposition of tilted dipole and quadrupole fields usually creates a very complex field structure which is difficult to analyze (e.g., Long et al. 2007, 2008). Consequently, for clarity we omit quadrupole fields in this work, re-

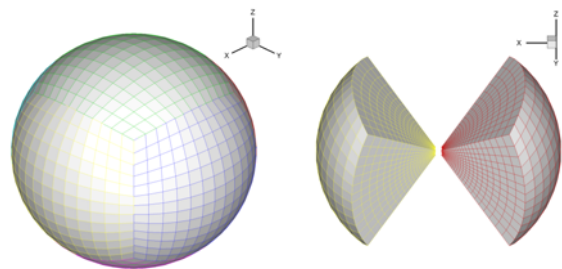


Figure 1: A low resolution “cubed sphere” grid is shown for demonstration. The left panel shows the grid on the surface of the inflated cube. Each of the six cube sides has $N^2 = 13^2$ curvilinear Cartesian grid cells. The grid consists of $N_r = 28$ concentric spheres. The right panel shows two sectors of the grid. Our simulations use a higher grid resolution, up to $N_r \times N^2 = 200 \times 51^2$ in each sector.

stricting our consideration to the clearer cases of a superposition of octupole and dipole fields, in order to focus on the role the octupole field plays in influencing the matter flow, the shapes of the resulting hot spots, and the light curves produced by these hot spots.

In separate papers, we investigated accretion onto CTTSs V2129 Oph and BP Tau, where the magnetic field configuration has been obtained from observations and is fixed (Romanova et al. 2011a; Long et al. 2011). In both cases, the octupolar component is not very strong relative to the dipole component. In this paper, we perform a systematic study of different combinations of the dipole and octupole components. In particular, we show our result for the case when the octupolar component strongly dominates.

Section 2 describes the simulation method and the magnetic field configurations. Section 3 presents our results for different combinations of dipole and octupole fields. Section 4 is devoted to the analysis of phase shifts in stars with complex fields. Section 5 summarizes and discusses our results.

2. Numerical model and magnetic field configurations

2.1. Model

Our 3D MHD model has been described in a series of papers (Koldoba et al. 2002; Romanova et al. 2003; 2004; Kulkarni & Romanova 2005; Long et al. 2007, 2008), where the disc accretion onto stars with dipole and more complex magnetic fields has been investigated. Here, we briefly summarize the different aspects of the model.

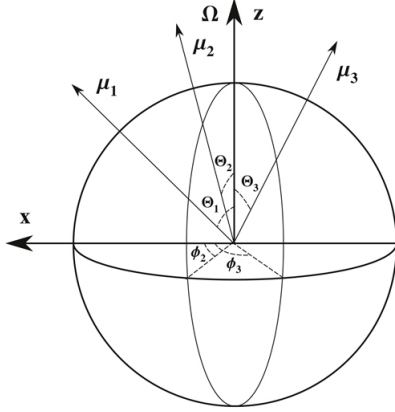


Figure 2: Sketch of the directions of the multipole magnetic moments. The rotation axis Ω is in the z direction. The magnetic axes of the dipole μ_1 , quadrupole μ_2 and octupole μ_3 are inclined at angles of Θ_1 , Θ_2 and Θ_3 from the z -axis. The dipole moment μ_1 is placed in the xz plane. The angles between $\Omega - \mu_2$, $\Omega - \mu_3$ and xz planes are ϕ_2 and ϕ_3 , respectively.

2.1.1. Dimensionless Variables and Reference Units

The MHD equations are solved using dimensionless variables \tilde{A} . To obtain the physical dimensional values A , the dimensionless values \tilde{A} should be multiplied by the corresponding reference units A_0 ; $A = \tilde{A}A_0$. To choose the reference units, we first choose the stellar mass M_\star and radius R_\star . The reference units are then chosen as follows: mass $M_0 = M_\star$, distance $R_0 = R_\star/0.35$, velocity $v_0 = (GM_0/R_0)^{1/2}$, time scale $P_0 = 2\pi R_0/v_0$, angular velocity $\Omega_0 = v_0/R_0$. The reference magnetic field B_0 can be obtained by choosing a reasonable fiducial value for the surface dipole field strength $B_{1\star}$. Then B_0 is the fiducial dipole field strength at R_0 ; $B_0 = B_{1\star}(R_\star/R_0)^3$. We then define the reference dipole moment $\mu_{1,0} = B_0 R_0^3$, quadrupole moment $\mu_{2,0} = B_0 R_0^4$, octupole moment $\mu_{3,0} = B_0 R_0^5$, density $\rho_0 = B_0^2/v_0^2$, pressure $p_0 = \rho_0 v_0^2$, mass accretion rate $\dot{M}_0 = \rho_0 v_0 R_0^2$, angular momentum flux $\dot{L}_0 = \rho_0 v_0^2 R_0^3$, energy per unit time $\dot{E}_0 = \rho_0 v_0^3 R_0^2$ (the radiation flux J is also in units of \dot{E}_0), temperature $T_0 = \mathcal{R}p_0/\rho_0$, where \mathcal{R} is the gas constant, and the effective blackbody temperature $T_{\text{eff},0} = (\rho_0 v_0^3/\sigma)^{1/4}$, where σ is the Stefan-Boltzmann constant.

Therefore, the dimensionless variables are $\tilde{r} = r/R_0$, $\tilde{v} = v/v_0$, $\tilde{t} = t/P_0$, $\tilde{B}_n = B_n/B_0$, $\tilde{\mu}_n = \mu_n/\mu_{n,0}$ ($n = 1, 2, 3$ for dipole, quadrupole and octupole components) and so on. In the subsequent sections, we show dimensionless values for all quantities and drop the tildes (\sim). Our dimensionless simulations are applicable to different astrophysical objects with different scales. We list the reference values for typical CTTs,

	CTTs	White dwarfs	Neutron stars
$M_\star (M_\odot)$	0.8	1	1.4
R_\star	$2R_\odot$	5000 km	10 km
$B_{1\star}$ (G)	10^3	10^6	10^9
R_0 (cm)	4×10^{11}	1.4×10^9	2.9×10^6
v_0 (cm s^{-1})	1.6×10^7	3×10^8	8.1×10^9
Ω_0 (s^{-1})	4×10^{-5}	0.2	2.8×10^3
P_0	1.8 days	29 s	2.2 ms
B_0 (G)	43	4.3×10^4	4.3×10^7
ρ_0 (g cm^{-3})	7×10^{-12}	2×10^{-8}	2.8×10^{-5}
p_0 (dy cm^{-2})	1.8×10^3	1.8×10^9	1.8×10^{15}
$\dot{M}_0 (M_\odot \text{yr}^{-1})$	2.8×10^{-7}	1.9×10^{-7}	2.9×10^{-8}
\dot{L}_0 ($\text{g cm}^2 \text{s}^{-2}$)	1.15×10^{38}	4.9×10^{36}	4.5×10^{34}
T_0 (K)	1.6×10^6	5.6×10^8	3.9×10^{11}
\dot{E}_0 (erg s^{-1})	4.8×10^{33}	1.2×10^{36}	1.2×10^{38}
$T_{\text{eff},0}$ (K)	4800	3.2×10^5	2.3×10^7

Table 1: Sample reference units for typical CTTs, cataclysmic variables, and millisecond pulsars. Real dimensional values for variables can be obtained by multiplying the dimensionless values of variables by these reference units.

cataclysmic variables, and millisecond pulsars in Tab. 1.

2.1.2. Initial Conditions

We consider a rotating magnetic star surrounded by an accretion disc and a corona. The disc is cold and dense, while the corona is hot and rarefied, and at the reference point (the inner edge of the disc in the disc plane), $T_c = 100T_d$, $\rho_c = 0.01\rho_d$, where the subscripts ‘d’ and ‘c’ denote the disc and the corona. The disc and corona are initially in rotational hydrodynamic equilibrium, where the sum of the gravitational, centrifugal, and pressure gradient forces is zero at each point in the simulation region. To avoid initial magnetic field discontinuity at the disc-corona boundary, the corona is set to rotate with the Keplerian angular velocity at each cylindrical radius r . An α -type viscosity is incorporated into the code. It operates only in the disc (above some density level, $\rho \gtrsim 0.2$) and helps regulate the accretion rate. We use a small value of $\alpha = 0.02$ for the majority of our simulation runs, and we use $\alpha = 0.04$ for the cases where the octupole field strongly dominates.¹ Other parameters of the disc such as the density distribution and initial structure are fixed in all of the simulations.

¹Note that the cases with dominantly octupolar fields are the most difficult to model, and the simulations do not last long. Somewhat faster-accreting disks helped to simulate these difficult cases over longer time scales.

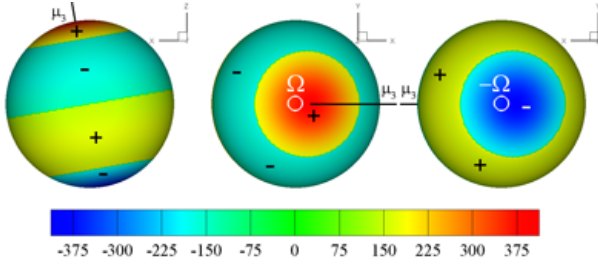


Figure 3: The magnetic field distribution on the star with an octupole field, $\mu_3 = 0.2$, $\Theta_3 = 5^\circ$, as seen from the equatorial plane (left panel), the north pole (middle panel) and the south pole (right panel).

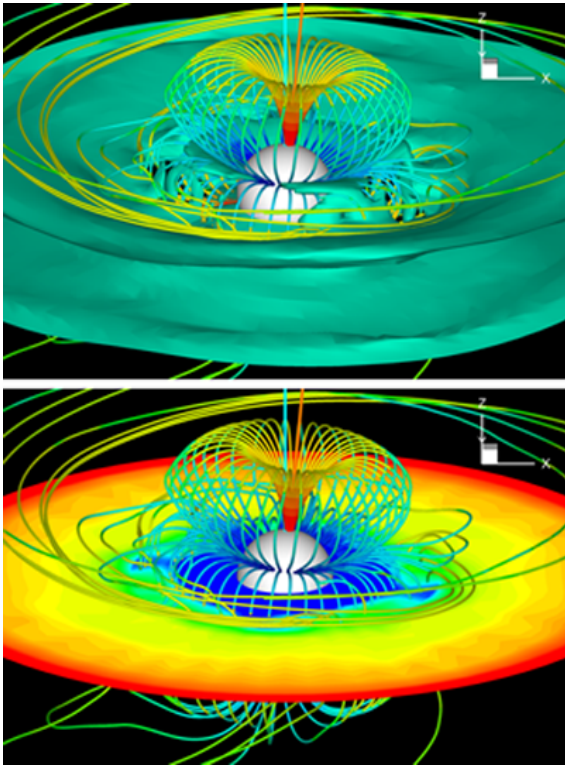


Figure 4: 3D views of matter flow to a star with an octupolar field with $\mu_3 = 0.2$, $\Theta_3 = 5^\circ$ at $t = 4.5$. The disc is shown by a constant density surface in green with $\rho = 0.15$ in the top panel. Different density levels in the equatorial plane are shown in the bottom panel. The colors along the field lines represent different polarities and strengths of the field. The thick cyan and orange lines represent the rotation and octupole moment axes, respectively.

2.1.3. Boundary Conditions

At the inner boundary (the surface of the star), most A variables are set to have free boundary conditions, $\partial A / \partial r = 0$. The initial magnetic field on the surface of the star is taken to be a superposition of tilted dipole and octupole fields (see B_1 and B_3 in Eqn. 2). As the simulation proceeds, we assume that the normal components of the fields remain unchanged, i.e., the magnetic field is frozen at the surface of the star. We neglect possible changes in the magnetic field structure inside the star due to, e.g., dynamo processes, because in most cases the time scale of such variations is much longer than the length of the simulation time. Our simulations last for 5 – 50 Keplerian rotations at the inner disc; the longest runs correspond to the dipole-dominated cases, while the shortest run corresponds to a purely octupolar case, which is numerically challenging.

The outer boundary is located at a radius of $r_{max} \approx 36R_\star$. The simulation region is large enough and the disc is massive enough to supply matter for the entire duration of the simulations. At the outer boundary, free conditions are taken for all variables. In addition, matter is not permitted to flow back from the outer boundary back into the simulation region.

2.1.4. The “Cubed sphere” Grid

The 3D MHD equations are solved with a Godunov-type code on the “cubed sphere” grid (Koldoba et al. 2002; see also Putman & Lin 2007). The grid consists of N_r concentric spheres, where each sphere represents an inflated cube. Fig. 1 shows that the grid consists of six sectors corresponding to six sides of the cube with $N \times N$ curvilinear Cartesian grids on each side. The whole grid consists of $6 \times N_r \times N^2$ cells. For modeling the octupole fields, a higher radial grid resolution is needed near the star compared with the pure dipole cases. We accomplish this by choosing the radial size of the grid cells to be 2.5 times smaller than the angular size in the region $r < (4 - 6)R_\star$ (see §2.1.1), while it is equal to the angular size in the outer region as in all our previous work. The typical grid used in simulations has $6 \times N_r \times N^2 = 6 \times 200 \times 51^2$ grid cells. Simulations with higher/lower grid resolutions were performed for comparisons.

2.2. Magnetic Field Configurations

When electrical currents outside the star can be neglected, the magnetic field there can be described by a magnetic scalar potential $\varphi(\mathbf{r})$ and can be represented as a sum of multipoles. The first three multipoles can be written as

$$\mathbf{B}(\mathbf{r}) = \mathbf{B}_1 + \mathbf{B}_2 + \mathbf{B}_3, \quad (1)$$

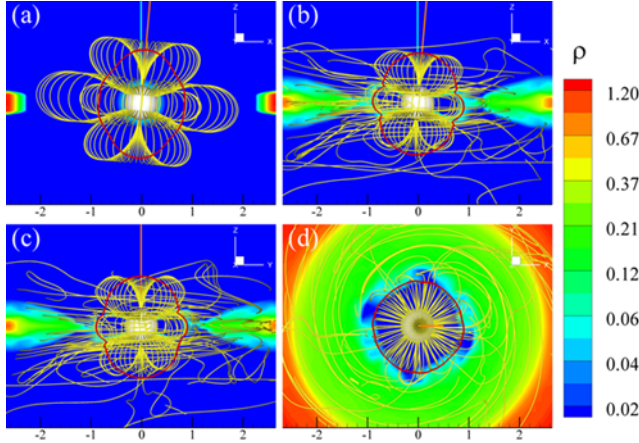


Figure 5: The density distribution in different planes (color background) and 3D magnetic field lines (yellow lines) for an octupole configuration with $\mu_3 = 0.2$, $\Theta_3 = 5^\circ$. Panel (a) shows an xz slice at $t = 0$; panels (b), (c) and (d) show xz , yz and xy slices at $t = 4.5$. The red lines show surfaces where $\beta_1 = 1$. The thick cyan and orange lines represent the rotation and octupole moment axes respectively.

where

$$\begin{aligned} \mathbf{B}_1 &= \frac{3\mu_1(\hat{\mu}_1 \cdot \hat{\mathbf{r}})}{r^3} \hat{\mathbf{r}} - \frac{\mu_1}{r^3} \hat{\mu}_1 \\ \mathbf{B}_2 &= \frac{3\mu_2}{4r^4} (5(\hat{\mu}_2 \cdot \hat{\mathbf{r}})^2 - 1) \hat{\mathbf{r}} - \frac{3\mu_2}{2r^4} (\hat{\mu}_2 \cdot \hat{\mathbf{r}}) \hat{\mu}_2 \\ \mathbf{B}_3 &= 5 \left(\frac{\mu_3}{2r^5} \right) (\hat{\mu}_3 \cdot \hat{\mathbf{r}}) [7(\hat{\mu}_3 \cdot \hat{\mathbf{r}})^2 - 3] \hat{\mathbf{r}} \\ &\quad - 3 \left(\frac{\mu_3}{2r^5} \right) [5(\hat{\mu}_3 \cdot \hat{\mathbf{r}})^2 - 1] \hat{\mu}_3. \end{aligned} \quad (2)$$

Here \mathbf{B}_1 , \mathbf{B}_2 , and \mathbf{B}_3 are the magnetic fields produced by the symmetric dipole, quadrupole and octupole moments and $\hat{\mathbf{r}}$, $\hat{\mu}_1$, $\hat{\mu}_2$, and $\hat{\mu}_3$ are the unit vectors describing the position and the symmetric dipole, quadrupole, and octupole moments, respectively. The magnetic moments may be inclined at angles Θ_1 , Θ_2 , and Θ_3 relative to the rotation axis Ω . They may also be in different meridional planes $\Omega - \mu_2$ and $\Omega - \mu_3$, with an azimuthal angles ϕ_2 and ϕ_3 relative to the $\Omega - \mu_1$ plane defined by the dipole moment and the rotation axis. Fig. 2 illustrates the geometry by an example in which all three magnetic moments have different orientations. For our simulations, we take only the dipolar and octupolar components and investigate the role of the octupolar component.

2.3. The Alfvén Surface and Magnetospheric Radius

The magnetospheric radius, r_m , is a characteristic radius where the inflowing matter is stopped by the magnetosphere. Several expressions for this radius have been derived since the 1970s for stars with dipole

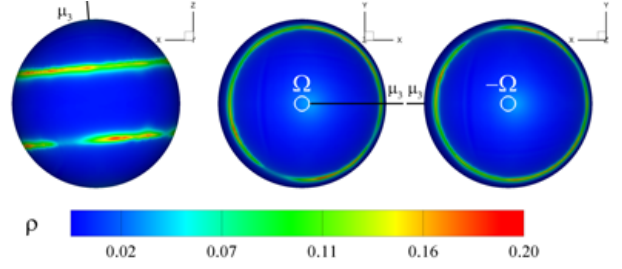


Figure 6: The surface density distribution on the star with an octupole magnetic field, $\mu_3 = 0.2$, $\Theta_3 = 5^\circ$, as seen from the equatorial plane (left panel), the north pole (middle panel), and the south pole (right panel).

fields. The first estimations were done for spherically-accreting matter. It was suggested that the radially-falling matter is stopped by the magnetic pressure of the magnetosphere (e.g., Lamb et al. 1973):

$$B(r_A)^2/8\pi = \rho(r_A)v(r_A)^2, \quad (3)$$

$$r_A = kr_A^{(0)}, \quad r_A^{(0)} = \dot{M}^{-2/7} \mu_1^{4/7} (GM)^{-1/7}, \quad (4)$$

where r_A is the Alfvén radius and k is a dimensionless coefficient on the order of unity (Elsner & Lamb 1977; Ghosh et al. 1977). For *disc* accretion, a similar criterion can be used but for stresses. The disc rotates in the azimuthal direction and hence main stresses are connected with the azimuthal components of the stress tensor: $T_{\phi\phi} = [p + \rho v_\phi^2] + [B^2/8\pi - B_\phi^2/4\pi]$ (here we neglected the viscous stress which is much smaller than the matter stress). The motion of the disc is disturbed by the rotating magnetosphere, when the matter stresses become comparable with the magnetic stresses, or $p + \rho v_\phi^2 = B^2/8\pi - B_\phi^2/4\pi$. The dominant component of the dipole magnetic field is the poloidal component, and hence $B_\phi \ll B$ and we obtain the condition for stresses as $p + \rho v_\phi^2 = B^2/8\pi$.

Different criteria were proposed by other authors (Collier Cameron & Campbell 1993; Armitage & Clarke 1996; Matt & Pudritz 2005). Analysis of these criteria shows that most of them give a radius similar to that given by Eqn. 4, but with different coefficients k (Bessolaz et al. 2008). A comparison of that formula with simulations gives $k \approx 0.5$ (Long, Romanova & Lovelace 2005), which is very close to the coefficient estimated by Ghosh & Lamb (1979).

For multipolar fields, we use the generalized formula, such that the n -th component of the field is $B_n \sim \mu_n/r^{n+2}$, (see details in Appendix Appendix A.2), and the magnetospheric radius

$$r_m = k_n r_{m,n}^{(0)}, \quad r_{m,n}^{(0)} = \mu_n^{4/(4n+3)} \dot{M}^{-2/(4n+3)} (GM)^{-1/(4n+3)}. \quad (5)$$

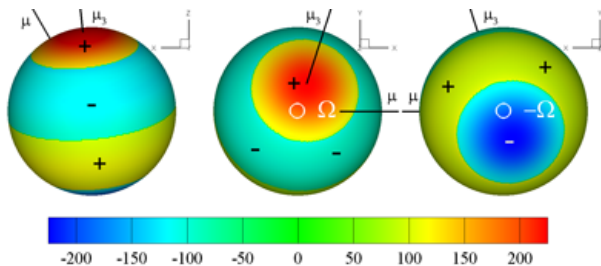


Figure 7: The magnetic field distribution on the star with a strong octupole and a weak dipole component, $\mu_1 = 0.2$, $\mu_3 = 0.3$, $\Theta_1 = 30^\circ$, $\Theta_3 = 20^\circ$, $\phi_3 = 70^\circ$, as seen from the equatorial plane (left panel), the north pole (middle panel) and the south pole (right panel).

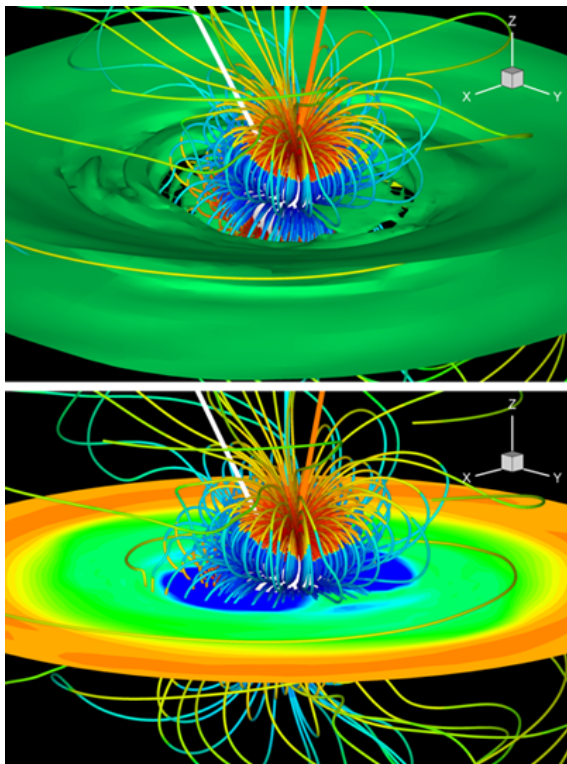


Figure 8: 3D views of matter flow to a star with a strong octupole and weak dipole magnetic field, $\mu_1 = 0.2$, $\mu_3 = 0.3$, $\Theta_1 = 30^\circ$, $\Theta_3 = 20^\circ$, $\phi_3 = 70^\circ$, at $t = 5$. The disc is shown by a constant density surface in green with $\rho = 0.2$ in the top panel; different density levels in the equatorial plane are shown in the bottom panel. The colors along the field lines represent different polarities and strengths of the field. The thick cyan, white and orange lines represent the rotation, dipole and octupole axes respectively.

3. Accretion onto Stars with an Octupole and a Dipole Field

In all of our simulations, we take a disc with the same initial density and pressure distribution. Then, we choose magnetic configurations with different strengths of the dipole and octupole fields, such that the disc is stopped either by the octupolar component of the field (in octupole-dominated cases), by the dipole component (in dipole-dominated cases), or by the dipole and octupole components of comparable strengths. We discuss these cases below in detail.

3.1. Pure octupole

First, we consider accretion onto a star with an octupole magnetic field with $\mu_3 = 0.2$. The magnetic axis of the octupole field is tilted relative to the stellar spin axis at a small angle, $\Theta_3 = 5^\circ$.

Fig. 3 shows the magnetic field distribution on the stellar surface. There are two polar regions with strong positive (red) and negative (blue) polarities, as seen in the middle and right panels. There are also two octupolar belts with opposite polarities as seen in the left panel. A meridian line which goes from the north to the south magnetic poles will pass through the positive northern pole, negative northern belt, positive southern belt and negative southern pole with zero magnetic field at the magnetic equator. This distribution differs from the dipole field which has only positive and negative poles.

Fig. 4 (top panel) shows 3D views of matter flow to the star at time $t = 4.5$. The magnetic field near the star has an octupolar shape with three sets of closed loops of field lines connecting regions of different polarities on the star, which we call *northern*, *southern* and *equatorial* sets of loops. Some field lines are closed, while others are dragged by the disc, wrapped around the rotation axis and inflate into the corona. Matter of the disc is lifted above the equatorial set of loops and flows into the northern magnetic belt on the star. The bottom panel shows the density distribution in the equatorial plane, where the disc matter is stopped by the equatorial set of loops and forms a low-density gap around the star.

Fig. 5 shows the density distribution in different planes and sample 3D magnetic field lines. Panel (a) shows that at $t = 0$ the magnetic field is a pure octupole field, where the three sets of loops of field lines are clearly seen. The equatorial set of loops is expanded to larger distances than the polar sets, to demonstrate the interaction of the magnetosphere with the disc. Panels (b) and (c) show that the disc matter is stopped by the magnetosphere, lifted above the disc plane and

channeled by the equatorial set of loops, before flowing into the octupolar belts on the stellar surface. Panel (b) shows that matter flow is not axisymmetric: more matter flows in from the direction towards which the octupole is inclined. Panel (d) shows that there is a low-density magnetospheric gap around the star.

The bold red line represents the magnetospheric surface, where the matter stresses equal the magnetic stresses,

$$\beta_1 = \frac{p + \rho v^2}{B^2/8\pi} = 1. \quad (6)$$

The magnetic field lines stay closed inside the magnetospheric surface, where the magnetic stresses dominate.

The initial octupolar field shown in panel (a) is a *potential* field, that is, a field that has not been disturbed by the surrounding plasma. The potential approximation is often used in extrapolation of the observed surface fields to larger distances (e.g., Jardine et al. 2002; Gregory et al. 2006; Donati et al. 2007). Panels (b)-(d) show that the potential approximation is sufficiently good inside the Alfvén surface, where $\beta_1 < 1$. However, the field strongly departs from the potential one at larger distances.

Fig. 6 shows that the hot spots on the stellar surface represent two rings which are located in the planes parallel to the magnetic equator. Each ring has a density enhancement on one side, where disc accretion is higher due to the inclination of the magnetic axis. The middle and right panels show that the density enhancements in the northern and southern rings are antisymmetric relative to the magnetic equatorial plane.

3.2. Strong octupole and weak dipole

Next, we consider the accretion onto a star with a superposition of a relatively strong octupole and a much weaker dipole component on the stellar surface: $\mu_1 = 0.2$, $\mu_3 = 0.3$, $\Theta_1 = 30^\circ$, $\Theta_3 = 20^\circ$, $\phi_3 = 70^\circ$. Here the rotation axis, dipole and octupole moments are all misaligned.

First, we estimate the radius at which the magnetic fields of the dipole and octupole components are equal. Using Eqn. 2, and suggesting for simplicity that the dipole and octupole moments are aligned, we obtain approximate formulae for the equatorial and polar magnetic fields: (1) Equatorial field: $B_1 = \mu_1/r^3$, $B_3 = (3/2)\mu_3/r^5$, and (2) Polar field: $B_1 = 2\mu_1/r^3$, $B_3 = 4\mu_3/r^5$. By equating B_1 and B_3 we obtain the distances where the dipole and octupole components are equal in the equatorial and polar directions:

$$r_{eq} = \left(\frac{3\mu_3}{2\mu_1}\right)^{\frac{1}{2}}, \quad r_{pole} = \left(\frac{2\mu_3}{\mu_1}\right)^{\frac{1}{2}}. \quad (7)$$

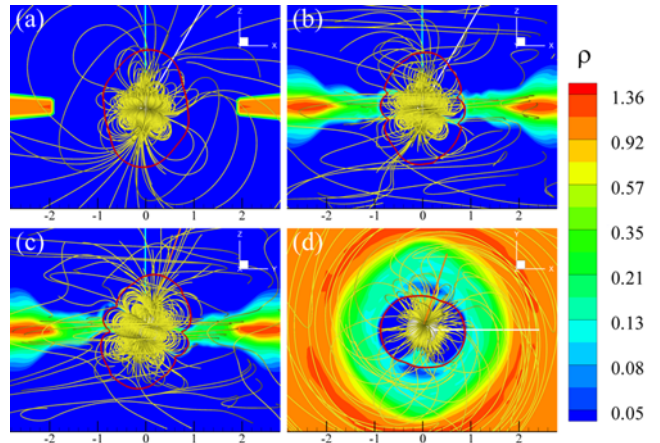


Figure 9: Density distribution in different slices (color background) and 3D magnetic field lines (yellow lines) for the case of an octupole plus weak dipole field with parameters $\mu_1 = 0.2$, $\mu_3 = 0.3$, $\Theta_1 = 30^\circ$, $\Theta_3 = 20^\circ$, $\phi_3 = 70^\circ$. Panel (a) shows an xz slice at $t = 0$; panels (b), (c), (d) show xz , yz and xy slices at $t = 5$. The red lines show the Alfvén surface, where $\beta_1 = 1$. The thick cyan, white and orange lines represent the rotation, dipole and octupole axes respectively.

Substituting for μ_1 and μ_3 , we obtain $r_{eq} = 1.5$ and $r_{pole} = 1.4$. At smaller/larger distances the octupole/dipole field dominates. It is evident that near the star, $r \sim R_\star = 0.35$, the octupolar component is much stronger than the dipole component. That is why in Fig. 7, the magnetic field distribution shows similar features to those in the pure octupole case (Fig. 3).

Fig. 8 shows 3D views of accretion flow onto the star at time $t = 5$. The disc matter comes close to the star and mainly interacts with the octupolar component and accretes onto the octupolar belts on the stellar surface. External field lines are dragged by the disc and inflate. This case shows similar features to that of the pure octupole, because in both cases the octupole determines matter flow. We should note that if the accretion rate were much smaller, then the inner disk would move to larger distances and the dipole component could interact with the disk. This case differs from that of a pure octupole field with no dipole component.

Fig. 9(a) shows that initially, at $t = 0$, the octupole component dominates near the star, while the dipole dominates at larger distances, such as the inner edge of the disc, which is different from the pure octupole case. Panels (b)-(d) show that the disc is stopped by the magnetosphere at $r_m \approx 0.9 \approx 2.6R_\star$. This radius is smaller than $r_{eq} \approx 1.5$, and therefore the octupolar field dominates at the disc-magnetosphere boundary. The accretion flow is similar to that in the pure octupole case (see Fig. 5), though here the misalignment angle $\Theta = 20^\circ$ is larger and matter flows more easily above the equa-

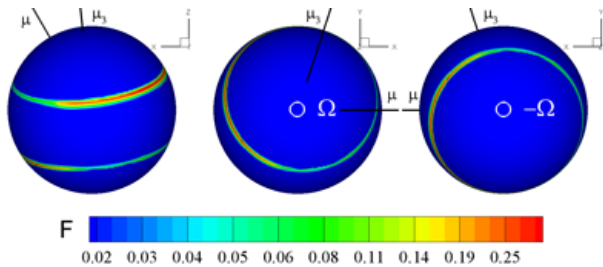


Figure 10: The energy flux distribution on the star with a strong octupole and weak dipole magnetic field, $\mu_1 = 0.2$, $\mu_3 = 0.3$, $\Theta_1 = 30^\circ$, $\Theta_3 = 20^\circ$, $\phi_3 = 70^\circ$, at $t = 5$, as seen from the equatorial plane (left panel), the north pole (middle panel), and the south pole (right panel).

torial set of loops. On the other hand, the octupole is inclined more strongly (than in the pure octupole case), and part of the funnel stream is located in the equatorial plane, due to which the magnetospheric gap is not empty (panel d). The red line in panel (d), $\beta_1 = 1$, shows that the matter stress equals the magnetic stress at $r \approx 1$, where the octupolar component dominates. At smaller accretion rates in the disk, the line moves to larger distances, and at $r \gtrsim 1.5$, the dipole component dominates.

Comparison of panel (a) with the other panels shows the difference between the initial potential field (panel a) and the non-potential fields obtained in the simulations. The magnetic field lines threading the disc and corona inflate, are wrapped around the rotation axis and form some kind of a magnetic tower (Romanova et al. 2011a). The field strongly differs from the potential one at $r > r_m$, where the disc and corona matter strongly disturb the magnetosphere. However, inside the magnetospheric radius, $r < r_m$, the magnetic stress dominates, and hence the magnetosphere is not disturbed by the plasma flow, and the potential approximation is valid.

For the calculation of the light curves, we use the same approach as Romanova et al. (2004). The total energy of the accreting matter is assumed to be converted into isotropic blackbody radiation on the surface of the star. The specific intensity of radiation from a position \mathbf{R} on the stellar surface into a solid angle $d\Omega$ in the direction $\hat{\mathbf{k}}$, is $I(\mathbf{R}, \hat{\mathbf{k}}) = (1/\pi)F(\mathbf{R})$, where $F(\mathbf{R})$ is the total energy flux of the inflowing matter, $\theta = \arccos(\hat{\mathbf{R}} \cdot \hat{\mathbf{k}})$. Therefore we obtain the radiation energy received per unit time in the direction $\hat{\mathbf{k}}$, $J = r^2 F_{obs} = \int I(\mathbf{R}, \hat{\mathbf{k}}) \cos \theta dS$, where r is the distance between the star and the observer, F_{obs} is the observed flux, and dS is the surface area element. Simulations show that, if the tilt of the dipole field is not very small ($\Theta \gtrsim 15^\circ$) and the accretion rate does not vary much with time, then the spots “choose” their favorite posi-

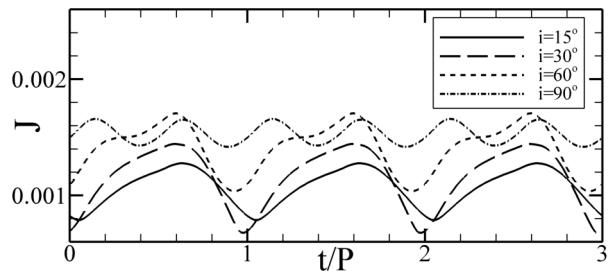


Figure 11: The light curves in the case of a strong octupole and a weak dipole, $\mu_1 = 0.2$, $\mu_3 = 0.3$ and $\Theta_1 = 30^\circ$, $\Theta_3 = 20^\circ$, $\phi_3 = 70^\circ$, for different inclination angles i .

tions on the surface of the star, where they vary a small amount (say, within 10°).² This is why we fix the spots at some moment of time and rotate the star to obtain the light curves.

Fig. 10 shows the distribution of the energy flux, F , on the surface of the star. The energy flux distribution is usually very similar to that of the density distribution. One can see that the spots in a purely octupolar case are similar to spots in this case. However, now the rings have a higher inclination relative to the equatorial plane due to the larger tilt of the octupolar axis (compared with the purely octupolar case).

Fig. 11 shows the light curves associated with the rotation of the star. The shapes of the light curves strongly depart from sinusoids, in contrast with the pure octupolar case. However, the cause is not the small dipole component, but instead the fact that the misalignment angle ($\Theta_3 = 20^\circ$) is larger than that in the pure octupolar case ($\Theta_3 = 10^\circ$), and a part of the southern ring is seen by the observer even at small inclination angles i . Each ring has a density (brightness) enhancement connected with the tilt, and these bright regions are in anti-phase (i.e., diametrically-opposite sides of the star). Hence, at small i , the observer mainly sees one ring, while only seeing part of the second ring, which gives one peak per period. At large i , the observer sees both rings in similar proportion, but the bright regions of rings alternate, and hence the light-curve has two peaks per period. See the animations for spots viewed at inclination angles $i = 0^\circ$ and $i = 90^\circ$ respectively.³

The above results are shown for the accretion rate determined in our code, in which the disk interacts with the octupolar component of the field. If the accretion

²In the opposite case of a smaller tilt and/or a highly variable accretion rate, a spot can change its position significantly; it can even rotate with its own angular velocity that is different from that of the star (Romanova et al. 2004, Bachetti et al. 2010).

³See Supplement: animations oct-dip-i0.avi and oct-dip-i90.avi.

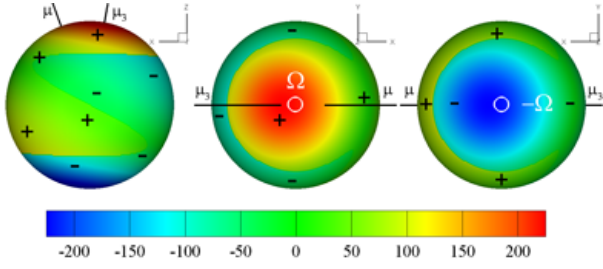


Figure 12: The surface magnetic field strength of a star with a strong dipole and weak octupole magnetic field, $\mu_1 = 2.0$, $\mu_3 = 0.2$, $\Theta_1 = 20^\circ$, $\Theta_3 = 10^\circ$, $\phi_3 = 180^\circ$, as seen from the equatorial plane (left panel), the north pole (middle panel) and the south pole (right panel).

rate decreases, then the inner disk will move to larger distances and the disk will start interacting with the dipolar component. This will lead to a different light-curve shape and to the phase shift in the light-curve equal to the phase difference between the dipolar and octupolar moments (see Sec. 4 for details).

3.3. Strong dipole and weak octupole

We now consider the case where the dipole component ($\mu_1 = 2.0$) is much stronger than the octupole component ($\mu_3 = 0.2$). The misalignment angles are $\Theta_1 = 20^\circ$, $\Theta_3 = 10^\circ$, the phase angle is $\phi_3 = 180^\circ$.

From Eqn. 7, we find the critical radii where the dipole and octupole components are equal: $r_{eq} = 0.39$ and $r_{pole} = 0.45$. These radii are only slightly larger than the radius of the star, $R_\star = 0.35$, and hence the dipole determines the dynamics of the flow in the entire vicinity of the star.

Fig. 12 shows the magnetic field on the surface of the star. The field distribution is complex and different from a dipole or octupole field. There are two magnetic poles with different polarities near the octupole axis, and two belts of different polarities caused by the octupole component. The field in the belts, however, is strongly distorted by the dipole component.

Fig. 13 shows the 3D views of the accretion flow to the star at $t = 9$. The magnetic field looks like a dipole at all distances. The matter is stopped by the dipole component of the magnetosphere and is channelled to the polar regions in two funnel streams, which is typical for accretion onto a star with a dipole field (Romanova et al. 2003). In the disc plane (bottom panel), the matter is stopped by the dipole-like field. One can see that the matter in the disc penetrates through the external layers of the magnetosphere due to the magnetic Rayleigh-Taylor instability which we often observe in 3D simulations (Romanova et al., 2008; Kulkarni & Romanova, 2008).

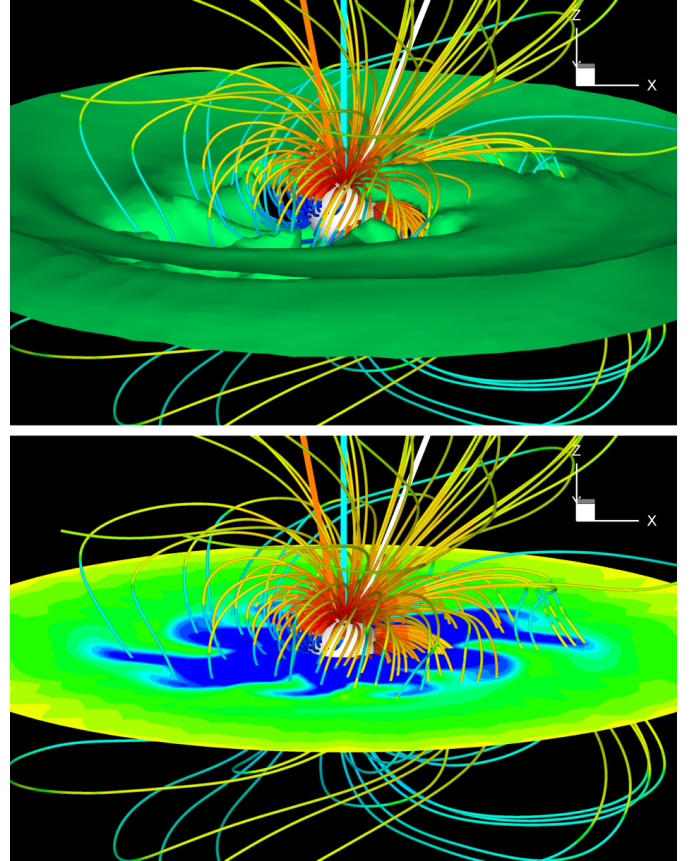


Figure 13: 3D views of matter flow to a star with a strong dipole and weak octupole magnetic field, $\mu_1 = 2.0$, $\mu_3 = 0.2$, $\Theta_1 = 20^\circ$, $\Theta_3 = 10^\circ$, $\phi_3 = 180^\circ$, at $t = 9$. The disc is shown by a constant density surface in green with $\rho = 0.25$ in the top panel; different density levels in the disc plane are shown in the bottom panel. The colors along the field lines represent different polarities and strengths of the field. The thick cyan, white and orange lines represent the rotation, dipole and octupole axes respectively.

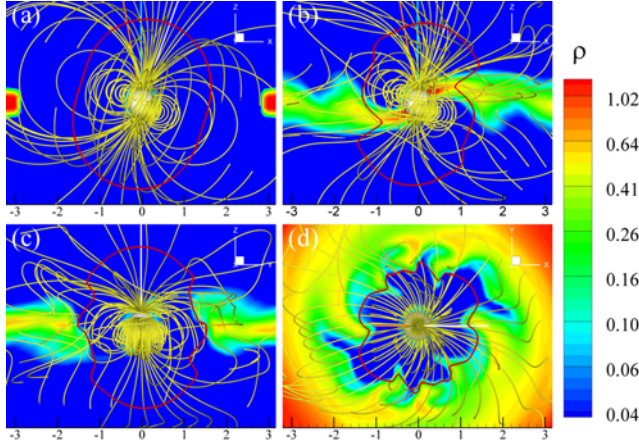


Figure 14: Density distribution in different slices (color background) and 3D magnetic field lines (yellow lines) for the case of a strong dipole and a very weak octupole field with parameters $\mu_1 = 2.0$, $\mu_3 = 0.2$, $\Theta_1 = 20^\circ$, $\Theta_3 = 10^\circ$, $\phi_3 = 180^\circ$. Panel (a) shows an xz slice at $t = 0$; panels (b), (c), (d) show xz , yz and xy slices at $t = 9$. The red lines show the magnetospheric surface, where $\beta_1 = 1$. The thick cyan, white and orange lines represent the rotation, dipole and octupole axes respectively.

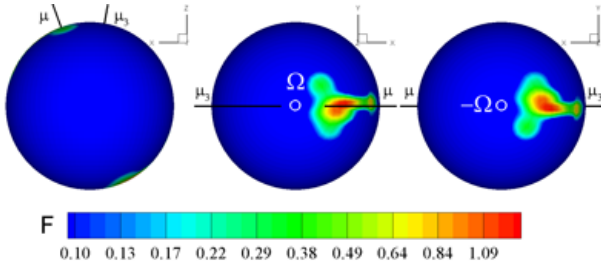


Figure 15: The hot spots viewed from different angles for the case of $\mu_1 = 2.0$, $\mu_3 = 0.2$, $\Theta_1 = 20^\circ$, $\Theta_3 = 10^\circ$, $\phi_3 = 180^\circ$: from the equatorial plane (left panel); from the north pole (middle panel); and from the south pole (right panel). The color represents the density.

Fig. 14 (panel a) shows that initially, at $t = 0$, the magnetic field has a dipole shape in the whole simulation region excluding the close vicinity of the star. Panels (b) and (c) show that the disc matter is stopped by the dipole-like magnetosphere and accretes towards the poles in two funnel streams. Panel (d) shows that a low-density magnetospheric gap forms around the star in the disc plane. Comparison of panel (a) with panels (b)-(d) shows that the potential approximation of the initially dipole magnetic field shown in panel (a) stays valid at later times only inside the magnetospheric surface, $r < r_m$, where $\beta_1 < 1$. At larger distances, the field lines are dragged by the disc and corona, and the field strongly departs from the initially potential dipole field.

The hot spots are shown in Fig. 15. As we expect,

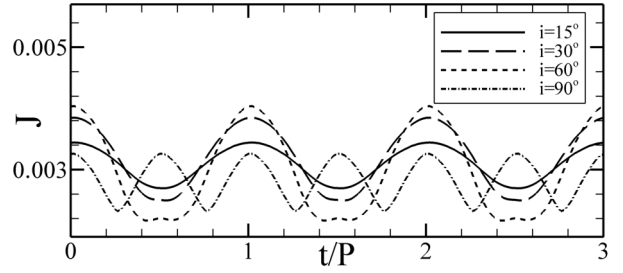


Figure 16: The light curves in the case of a strong dipole and weak octupole, $\mu_1 = 2.0$, $\mu_3 = 0.2$, $\Theta_1 = 20^\circ$, $\Theta_3 = 10^\circ$, $\phi_3 = 180^\circ$, for different inclination angles i .

there are only two polar spots, which is typical for accretion onto a star with a dipole field. No ring-like spots are observed because the dipole component dominates almost everywhere and matter is not channeled by the octupole-like field. The hot spots are located near the northern and southern magnetic poles. See our supplemental animations for spots viewed at inclination angles of $i = 0^\circ$ and $i = 90^\circ$, respectively.⁴

Fig. 16 shows the light curves associated with the rotation of the star at $t = 9$. The shapes of the light curves are quite sinusoidal for almost all inclination angles, which is also typical for stars with slightly tilted dipole fields (Romanova et al. 2004). At large i , two peaks per period are observed, because the spot near the southern magnetic pole becomes visible and contributes to the light curves.

3.4. Dipole and octupole of comparable strength

We now consider an interesting case where both dipole and octupole components disrupt the disc and channel matter. The parameters are: $\mu_1 = 1$, $\mu_3 = 0.3$, $\Theta_1 = 30^\circ$, $\Theta_3 = 20^\circ$, $\phi_3 = 70^\circ$. For these parameters we find from Eqn. 7: $r_{eq} = 0.67$, $r_{pole} = 0.77$. However, the inclination of the dipole and octupole axes could also influence the result. Fig. 17 shows a close view of the matter flow. In the xz plane, the funnel streams are first channeled by the dipole-like field. When the matter flows close to the star, at about $2R_\star$, the octupole determines the flow and converts each funnel stream into three small accretion streams between the loops of field lines. In the yz plane, the disc is stopped by the dipole component, and only a small amount of matter flows along the dipole-like field lines and is then governed by the octupole. The xy plane shows that matter flow is strongly non-axisymmetric: in some directions the disc

⁴See Supplement: animations dip-oct-i0.avi and dip-oct-i90.avi.

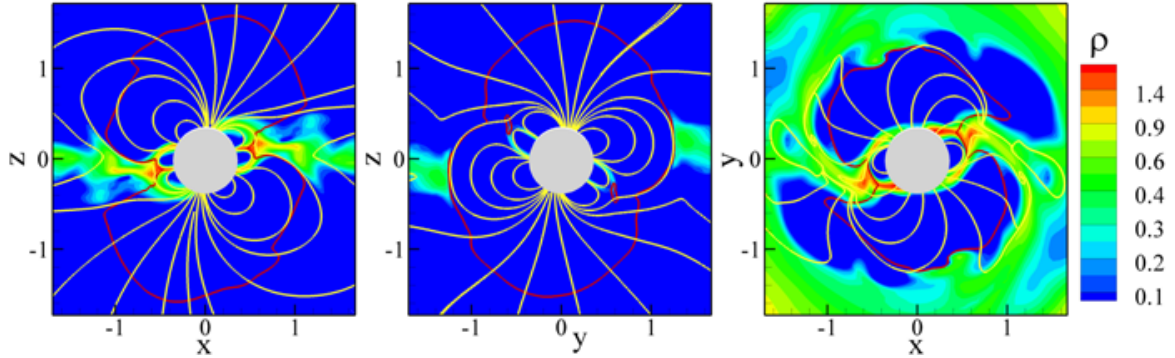


Figure 17: Close view of the density distribution in different slices (color background) and magnetic field lines (yellow lines) for the case of a strong dipole and octupole magnetic field with parameters $\mu_1 = 1.0$, $\mu_3 = 0.3$, $\Theta_1 = 30^\circ$, $\Theta_3 = 20^\circ$, $\phi_3 = 70^\circ$. From left to right: xz , yz and xy slices at $t = 3.5$. The red line shows the magnetospheric surface, where $\beta_1 = 1$.

matter is stopped by the dipole, and in other directions matter flows much closer to the star and is stopped by the octupolar component.

Fig. 18 shows the hot spots in this case. Most of the matter is governed by the octupolar field and forms ring-like spots. Some matter flows into the polar regions located near the dipole magnetic poles.

4. Phase shifts in light curves of stars with complex fields

Here, we consider the possible mechanisms causing phase shifts in the light-curves of stars with complex fields. We consider two main mechanisms. First, if the magnetic field of the star reconstructs, then this leads to a shift of the magnetic poles; second, if the accretion rate varies with time, then the disc interacts with different multipoles, which have different phases. Below, we discuss these two possibilities.

4.1. Phase shift due to field reconstruction

The magnetic field of a star may vary with time due to internal dynamo processes. Such variations may lead to a reconstruction of the field, and different multipoles may dominate after the reconstruction. Or, the reconstructed field may have the same multipoles, but with different orientations of their magnetic axes. Here we investigate an example where a predominantly octupolar field changes the orientation of its magnetic axis. We choose an octupole with $\mu_3 = 0.3$, which in state (a), has its magnetic axis at $\Theta_3 = 20^\circ$ and $\phi_3 = 70^\circ$. Later, in state (b), it has new orientation angles, $\Theta_3 = 60^\circ$ and $\phi_3 = 150^\circ$. In both cases we have a small dipole component: $\mu_1 = 0.2$, $\Theta_1 = 30^\circ$, which does not change.

We observe that in both cases the disc interacts with the octupole-like field close to the star (like in §3.1) and the hot spots represent two octupolar rings. However, the orientation of the rings and their brightness distribution are different due to the different axis directions. Most importantly, the octupole axes have different directions relative to the meridional plane, which leads to changes in hot spots and this, in turn, determines the phase shift. Fig. 19 shows that the light curves in states (a) and (b) have different phases with a phase shift of $\Delta\Phi = \Phi_b - \Phi_a = 170^\circ$, where the amplitudes are normalized to the same values. The shapes of the light curves are different because the angle Θ_3 is different in these states, although this difference may not always lead to changes in the pulse shapes.

In most cases it is not well known how fast the dynamo-driven magnetic field reconstruction is. Observations of the CTTSs type young stars show that possibly the field may vary on the scales of months or even weeks (Smirnov et al. 2004; Donati et al. 2008). What the time scales of magnetic field variations in neutron stars and white dwarfs are is less clear.

We should mention that such phase shifts could occur during the reconstruction of a field with any combination of multipoles, including a purely dipole configuration.

4.2. Phase shifts due to accretion rate variation

In another example we consider a star with a fixed complex field where the different multipoles are oriented at different meridional angles, ϕ_n . Then, at high accretion rates, the disc comes closer to the star and interacts with the higher order multipoles, while at lower accretion rates, the truncation distance of the disc moves away from the star and interacts with the lower order multipoles.

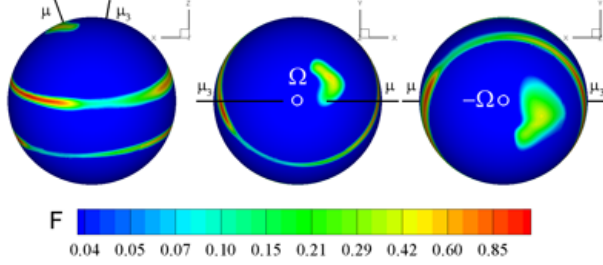


Figure 18: The hot spots viewed from different angles for the case of $\mu_1 = 1.0$, $\mu_3 = 0.3$, $\Theta_1 = 30^\circ$, $\Theta_3 = 20^\circ$, $\phi_3 = 70^\circ$: from the equatorial plane (left panel); from the north pole (middle panel); and from the south pole (right panel). The color represents the density.

To study this case, we need a slight reinterpretation of our reference units defined in §2.1.1. So far, we have used the *dimensionless* parameters μ_1 and μ_3 to control the magnetic moments of the star. However, they can also be used to control the accretion rate instead, which is more convenient in this subsection; all we need to do is recast the reference units into a different form. In order to do that, we note that the *dimensional* dipole moment of the star is $\mu_{1\star} = \mu_1 \mu_{1,0}$. In the previous sections, we kept the reference value $\mu_{1,0}$ fixed, which is why varying μ_1 corresponded to varying the dipole moment. Now, however, we keep $\mu_{1\star}$ fixed. It is then convenient to express $\mu_{1,0}$ in terms of $\mu_{1\star}$ as $\mu_{1,0} = \mu_{1\star}/\mu_1$. Then, $\mu_{1,0} = B_0 R_0^3$ gives $B_0 = \mu_{1,0}/R_0^3 = \mu_{1\star}/\mu_1 R_0^3$, and $\mu_{3,0} = B_0 R_0^5$ becomes $\mu_{3,0} = \mu_{1\star} R_0^2/\mu_1$. The dimensional octupole moment then is $\mu_{3\star} = \mu_3 \mu_{3,0} = (\mu_3/\mu_1) \mu_{1\star} R_0^2$. The reference accretion rate is $\dot{M}_0 = \rho_0 v_0 R_0^2 = B_0^2 R_0^{5/2} / \sqrt{GM} = \mu_{1\star}^2 / (\mu_1^2 R_0^{7/2} \sqrt{GM})$. The dimensional accretion rate \dot{M}_{dim} is then given by

$$\dot{M}_{dim} \approx \left(\frac{\dot{M}}{\mu_1^2} \right) \frac{\mu_{1\star}^2}{(GM_\star)^{1/2} R_0^{7/2}}. \quad (8)$$

It is now clear that changing the *dimensionless* parameter μ_1 has the effect of changing the accretion rate \dot{M}_{dim} , while keeping $\mu_{1\star}$ fixed as mentioned above. To keep $\mu_{3\star}$ fixed as well, we simply have to change μ_3 such that the ratio $\mu_{3\star}/\mu_{1\star}$ is fixed. This allows us to change the accretion rate while keeping the stellar magnetic field fixed.

The physical meaning of this recasting is the following. The most natural interpretation of changing μ_1 and μ_3 is changing the stellar magnetic field, the result of which is a decrease in the magnetospheric radius. However, we can also decrease the magnetospheric radius by fixing the stellar magnetic field and increasing the accretion rate instead, which is exactly what Eqn. 8 shows. The dimensionless parameters μ_1 and μ_3 are therefore best thought of as controlling the *magnetospheric size*.

This yields us the convenient possibility of using μ_1 to represent two states of a star with different accretion rates to investigate the phase shifts between them. As an example, we take a star with a superposition of dipole and octupole fields, where they have parameters, $\Theta_1 = 30^\circ$, $\Theta_3 = 20^\circ$, $\phi_3 = 70^\circ$ and fixed ratio of μ_3/μ_1 . It is important that the dipole and octupole have different phase angles ϕ_n .

We choose two states with the above parameters for the dipole and octupole, but with different μ_1 : state (a) with $\mu_1 = 2$; and state (b) with $\mu_1 = 0.2$. We observe from simulations that in state (a) the disc interacts mainly with the dipole component, while in state (b) it

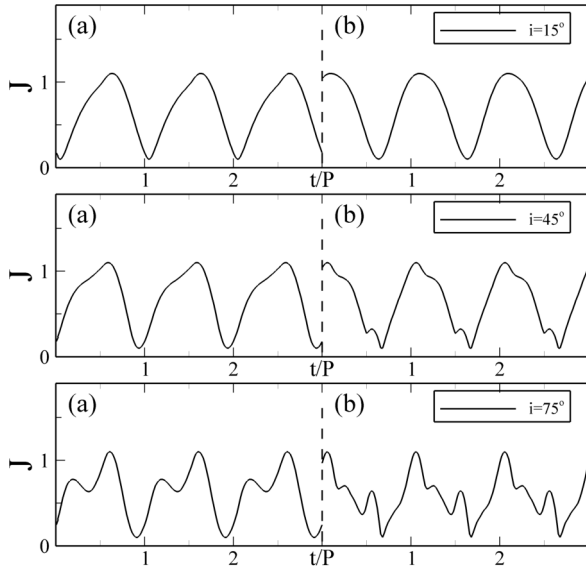


Figure 19: The phase shift due to the magnetic field reconstruction. The field is predominantly the octupolar field ($\mu_3 = 0.3$, $\mu_1 = 0.2$, $\Theta_1 = 30^\circ$), and the octupolar axis changes its orientation. In the state (a) $\Theta_3 = 20^\circ$ and $\phi_3 = 70^\circ$, in the state (b) $\Theta_3 = 60^\circ$ and $\phi_3 = 150^\circ$.

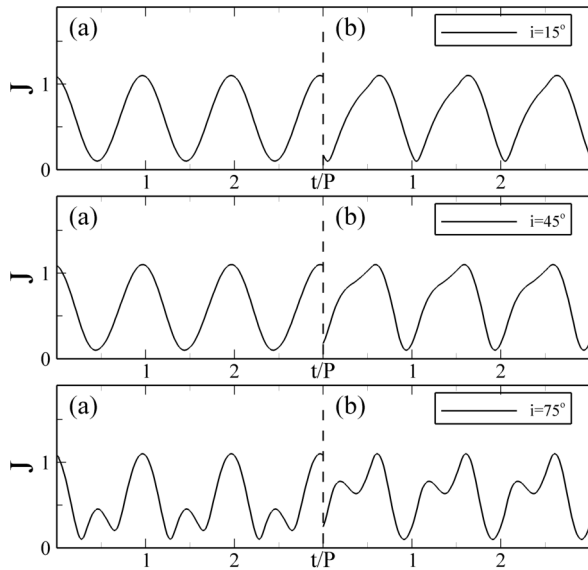


Figure 20: The phase shift due to the variation of the accretion rate. (a) For low accretion rate ($\mu_1 = 2$), the dipole component stops the disc. (b) For high accretion rate ($\mu_1 = 0.2$), the octupole component stops the disc. The phase shift occurs at the transition between these two states.

interacts mainly with the octupole component. Fig. 20 shows a phase shift of peaks $\Delta\Phi = \Phi_b - \Phi_a = 120^\circ$ between the states (a) and (b), where the amplitudes are normalized to the same values. The phase shift occurs because the octupole and dipole axes are located in different meridional planes and have different angles ϕ , due to which the matter flows to different places of the star at different accretion rates.

This type of phase shift is expected during periods of accretion rate variation. What is the accretion rate “jump” between states (a) and (b)? We can give a simple estimate, $(\dot{M})_b/(\dot{M})_a = ((\mu_1)_a/(\mu_1)_b)^2 = (2/0.2)^2 = 100$. However, we should notice that in state (b) the octupole strongly dominates and Eqn. 8 may not be used directly. In addition, the transition may occur at smaller values of μ_1 in state (a). So it is clear that this type of phase shift may be produced by accretion rate (luminosity) variation.

Another point that should be noted is that the phase shifts would be expected to be accompanied by changes in the light curve pulse profile, because the shape and position of the hot spots are very different at different field configurations.

5. Discussion of Phase Shifts in Accreting Millisecond Pulsars (AMPs)

Different types of phase shifts are observed in accreting millisecond pulsars, in which a weak neutron star magnetic field ($B \sim 10^8 - 10^9$ G) truncates the accretion disk at a distance of a few stellar radii, and in which the disk-magnetosphere interaction determines many of observational properties of the neutron star (e.g., Wijanands & van der Klis 1998; Chakrabarti & Morgan 1998). The main type of phase shift is connected with so-called *timing noise* which appears as irregular pulse-phase jumps on timescales from hours to months (e.g., Burderi et al. 2006; Hartman et al. 2008). The amplitude of pulse-phase offsets usually correlated with X-ray flux (e.g., Papitto et al. 2007; Reggio et al. 2008; Patruno et al. 2009a,b) though sudden strong jumps in phase are also observed (e.g., Burderi et al. 2006; Hartman et al. 2008, 2009). This phenomenon is not completely understood yet. The correlation of the pulse-phase offsets with X-ray flux may be an argument in favor of a “moving spots” model, in which the position of hot spots on the stellar surface depends on the accretion rate (Patruno et al. 2009a,b). Spot motions have been observed in 3D MHD simulations (Romanova et al. 2003, 2004) and have been proposed as an explanation of timing noise by Lamb et al. (2009a,b). This explanation is a possibility. Alternatively, we suggest that the phase shifts could be connected with the variation of the accretion rate for a star with a complex field, as discussed in Sec. 4.2. In this model, the phase shift is also proportional to the accretion rate, as in the moving spots model. More detailed analysis is required to decide between these two models.

The pulse shape usually varies during an outburst, and hence the contribution of different harmonics varies in time. This also leads to the timing noise (e.g., Poutanen et al. 2009; Gierlinsky & Poutanen 2005; Poutanen & Gierlinsky 2003). Moreover, there is a phase shift between the soft and hard X-ray bands, in which the pulse arrival in the soft X-ray band is lagging behind that in the hard X-ray band (Cui et al. 1998). This phenomenon can be connected with the details of radiation in the shock near the surface of the neutron star (Poutanen and Gierliński, 2003), and it adds complexity to the problem of timing noise (Gierliński and Poutanen, 2005). In our model of “complex fields + varying accretion rate”, the pulse shape also varies in time, which also might contribute to the timing noise. However, in our model, the phase jumps are usually not at the origin of pulse shape changes. This is different from the model proposed by, e.g., Poutanen et al. (2009), which

is focused on the pulse profile changes to investigate the origin of timing noise in accreting pulsars.

In another phase-shift model proposed in this paper (see Sec. 4.1), the phase shifts are connected with the magnetic field reconstruction due to the internal processes in the star. In this case, the phase shifts (or jumps) are expected to be random and occur with no correlation with the X-ray flux. This mechanism is definitely expected in some accreting young solar-type stars, in which the magnetic field varies rapidly due to convection processes inside the star (e.g., Donati et al. 2010). It is less clear whether this mechanism operates in accreting neutron stars. The magnetic field of *isolated* millisecond pulsars varies only slowly in time due to slow processes in the liquid core of the neutron star (e.g., Ruderman 1991) or due to slow diffusion of the earlier buried magnetic field through the crust of the neutron star (e.g., Cumming, Zweibel & Bildsten 2001). In both cases, it is expected that the global field of millisecond pulsars varies on time-scales that are much longer than the observed bursts. However, the situation can be different in cases of presently-accreting millisecond pulsars, in which temporarily enhanced accretion events can lead to temporary burial of parts of the stellar magnetic flux, which can diffuse back much faster. Accretion through the funnel streams leads to enhanced accretion towards the magnetic poles (Lovelace, Romanova & Bisnovatyi-Kogan 2005) and to formation of temporary polar ‘mountains’ at the poles (Payne & Melatos 2004, 2006), while the magnetic flux is pushed towards the equator. This field will be redistributed at later times, after a thermonuclear burst. Another possibility for the temporary redistribution of the field has been observed in global simulations of disk-magnetosphere interactions, in which the accretion disk reaches the surface of the star during periods of high accretion rate. Simulations show that, in cases of very high accretion rates, the disk matter accretes through the equatorial boundary layer, and it pushes parts of the field towards the stellar surface⁵. We suggest that this field can be temporarily buried by the accreting matter, and then it will diffuse out relatively fast. Such a situation can be realized during the maximum point of the outburst, which is when the disk can reach the surface of the star. Subsequently, the field will reconstruct relatively fast due to diffusion through a thin layer of accreted matter. Reconstruction of this field will lead to the phase jumps which would be observed on the background of

⁵Global simulations show that the magnetic field is strongly modified during equatorial accretion; it looks like a quadrupolar or more complex field (see, e.g., fig. 15 of Romanova et al. 2011b)

the gradually declining X-ray flux. Of course, this possibility should be investigated further.

We should also note that in the model where the phase varies due to variation of the accretion rate, the phase is expected to return back to its original value, as soon as the accretion rate returns back. However, in the model where the field reconstructs in time, the phase will not return back.

6. Conclusions and discussion

We performed global 3D MHD simulations of accretion onto stars with predominantly octupolar magnetic fields, and for a combination of dipole and octupole fields. The calculation became possible due to the enhancement of the grid resolution near the star. Simulations have shown that:

1. If the disc interacts predominantly with the octupolar field, then matter flows into two octupolar rings on the surface of the star. In the case of an inclined octupole field, the hot spots are inclined and have a brightness amplification on one side of the ring. At small tilt angles of the octupole, $\Theta = 10^\circ$, the light curves are quite sinusoidal and “mimic” the shape of the light curves of the pure dipole field, in particular at small inclination angles i . However, at larger Θ (e.g., $\Theta = 20^\circ$), the light curves strongly depart from sinusoidal, even for small i .
2. If the dipole component strongly dominates, then matter flows in two funnel streams governed by the dipole field, and two round spots form in the vicinity of the dipole magnetic poles. If the dipole and octupole have comparable strengths at the truncation radius, then both components channel matter to the star. Usually both octupolar rings and polar spots form on the surface of the star.
3. The potential field approximation is valid only in the region around the star where the magnetic stresses are higher than the matter stresses. At larger distances, the field is dragged by the disc and corona and strongly departs from being potential. The external magnetic field usually acquires a significant azimuthal component and inflates. A number of field lines wrap around the rotation axis, forming a magnetic tower which may propagate to larger distances due to magnetic force (e.g., Romanova et al. 2011a).
4. Accretion onto stars with multipolar fields may lead to phase shifts in the light curves. This may occur in the following situations: (a) If the complex magnetic field is fixed but the accretion rate

varies, then the disk interacts with multipoles of different orders that may have different tilts, θ_n , and phase angles, ϕ_n . These phase-shifts will correlate with the variation of the accretion rate. (b) If the magnetic field of the star varies in time due to, e.g., dynamo process (in young stars) or due to some other processes (e.g., temporary burial of the field in compact stars), then the phase-shifts will be connected with reconstruction of the field and motion of magnetic poles. It is expected that the pulse profiles will vary during these phase-shifts, because the shapes and positions of the hot spots are different in different field configurations.

These new challenging 3D simulations helped us to understand the nature of accretion onto stars with octupolar fields. Recent measurements by Donati et al. (2007, 2008) of the two CTTSs V2129 Oph and BP Tau have shown that their fields have a significant octupolar component. In our next papers (Romanova et al. 2011a; Long et al. 2011) we compare our numerical model with observations of these stars.

Magnetic fields in young, T Tauri-type stars, may have a complex structure and may vary with time due to internal dynamo processes. The recently measured magnetic fields of CTTS stars CV Cha and CR Cha (Hussain et al. 2009) show a complex structure consisting of a number of multipoles. In another CTTS, V2247 Oph, the magnetic field is complex and varies on the time-scale of weeks (Donati et al. 2010; see also Smirnov et al. 2005; Donati et al. 2011). Frequent phase shifts are expected in this star due to internal field reconstruction, as discussed in this paper. In all these stars the phase shifts may also occur due to accretion rate variations and interactions with different multipoles.

Photometric variability of CTTSs show complex patterns and are still puzzling (e.g., Herbst et al. 1994; Percy, Gryc & Wong 2006; Grankin et al. 2007). It is often the case that, instead of a definite period, a quasi-period is observed, and its frequency varies with time (e.g., Alencar & Batalha 2002; Rucinski et al. 2008). This may be connected with the phase-shift of the main period, in which the period varies on a time-scale of the rotation of the star. This phenomenon of phase-shifts should be further investigated.

Phase-shifts are observed in millisecond pulsars, and we discuss possible application of our models to these objects in Sec. 5. Similar phase-shifts are expected in accreting, weakly-magnetized white dwarfs (e.g., Dwarf Novae or in Intermediate Polars).

Acknowledgments

This research was conducted using the NASA High End Computing Program computing systems, specifically the Columbia, Discover and Pleiades superclusters. The authors thank A.V. Koldoba and G.V. Ustyugova for the earlier development of the codes, and A.A. Blinova, A.K. Kulkarni and R.V.E. Lovelace for helpful discussions. The research is supported by NSF grant AST0709015, and funds of the Fortner Endowed Chair at Illinois. Research of MMR is supported by NASA grant NNX08AH25G and NSF grant AST-0807129.

Appendix A. The magnetospheric radius

The magnetospheric radius r_m is the radius where the disc is truncated by the magnetosphere. It is also used to depict the characteristic size of the magnetosphere. Here we estimate the magnetospheric radii for various multipoles. For simplicity we assume that they are aligned with the rotation axis.

Appendix A.1. The Magnetospheric Radius for A Dipole Field

Here we derive the general formula for the truncation (magnetospheric) radius r_m in the cases of the dipole fields. The disc is truncated where the magnetic stresses equal the matter stresses, $B^2/8\pi = p + \rho v_\phi^2$. We assume that the disc is cold, $p \ll \rho v_\phi^2$, hence $B^2/8\pi = \rho v_\phi^2$.

We also assume that the system is in a stationary state and matter is supplied from the viscous disc with a constant accretion rate $\dot{M} = 4\pi r h v_r \rho$, where r is the distance to the star, $h = (c_s/v_K)r$ is the disc scale height, $v_r = \alpha c_s^2/v_K$ is the radial flow velocity, c_s is the sound speed, $v_K = (GM/r)^{1/2}$ is the Keplerian velocity, α is the Shakura-Sunyaev viscosity parameter. We obtain,

$$\rho v_\phi^2 \approx \rho v_K^2 = (4\pi\alpha)^{-1} (v_K/c_s)^3 \dot{M} (GM)^{1/2} r^{-5/2}. \quad (\text{A.1})$$

For the equatorial component of the *dipole field* the magnetic field is $B = \mu_1/r^3$. Substituting into the equation $B^2/8\pi = \rho v_\phi^2$ and using Eqn. A.1, we obtain,

$$r_m = k_1 r_m^{(0)}, \quad k_1 = (\alpha^2/2)^{1/7} (c_s/v_K)^{6/7}, \quad (\text{A.2})$$

$$r_m^{(0)} = \mu_1^{4/7} \dot{M}^{-2/7} (GM)^{-1/7}.$$

The main term, $r_m^{(0)} = \mu_1^{4/7} \dot{M}^{-2/7} (GM)^{-1/7}$, exactly coincides with the main term for spherical accretion (see also Bessolaz et al. 2008). However, here the coefficient k_1 depends on α and the ratio c_s/v_K . We should note that the formula for \dot{M} used in this derivation is applicable only for thin discs, and is only approximately

valid near the magnetosphere, where the disc matter is accumulated, the disc becomes thicker and has an excess of matter pressure. That is why the coefficient k_1 can be considered to be approximate and can be substituted with some number. Comparison of numerical results for r_m with Eqn. A.2 made in Long et al. (2005) shows that for their set of simulations, $k_1 \approx 0.5$ (see more comparisons in Bessolaz et al. 2008).

Appendix A.2. The Magnetospheric Radius for A Multipolar Field

Next, we derive the magnetospheric radius for multipolar field. For simplicity, we assume that the main axis of the multipolar field is *aligned* with the rotation axis, and therefore the n -th multipolar component of the magnetic field can be presented in the form $B_n \sim \mu_n/r^{n+2}$. Similarly, we obtain,

$$r_{m,n} = k_n r_{m,n}^{(0)}, \quad k_n = (\alpha^2/2)^{\frac{1}{4n+3}} (c_s/v_K)^{\frac{6}{4n+3}},$$

$$r_{m,n}^{(0)} = \mu_n^{\frac{4}{4n+3}} \dot{M}^{-\frac{2}{4n+3}} (GM)^{-\frac{1}{4n+3}}. \quad (\text{A.3})$$

This formula can be applied in the cases of aligned multipoles, or can be used for estimates of the magnetospheric radius in general, misaligned cases.

We should note that the B_z equals 0 in the disc plane for aligned fields of $2n$ -th order multipoles, such as quadrupole (ref. Long et al. 2007), and matter could flow directly to the star in the disc plane. So $r_{m,n}$ does not reflect where the inflowing matter stops, but only the size of magnetosphere.

References

Alencar S. H. P., Batalha C., 2002, ApJ, 571, 378
 Armitage P. J., Clarke C. J., 1996, MNRAS, 280, 458
 Bachetti, M., Romanova, M. M., Kulkarni, A., Burderi, L., di Salvo, T., 2010, MNRAS, 403, 1193
 Basri G., Marcy G. W., Valenti J. A., 1992, ApJ, 390, 622
 Beuermann K., Euchner F., Reinsch K., Jordan S., Gänsicke B. T., 2007, A&A, 463, 647
 Bessolaz N., Zanni C., Ferreira J., Keppens R., Bouvier J., 2008, A&A 478, 155
 Bignami, G. F., Caraveo, P. A., De Luca, A., Mereghetti, S., 2003, Nature, 423, 725
 Burderi L., Di Salvo T., Menna, M.T., Riggio, A., & Papitto, A. 2006, ApJ, 635, L133
 Burderi L., Di Salvo T., Robba N. R., La Barbera A., Guainazzi M., 2000, ApJ, 530, 429
 Chakrabarty, D., & Morgan, E.H. 1998, Nature, 394, 346
 Cumming, A., Zweibel, E., Bildsten, L. 2001, ApJ, 557, 958
 Coburn, W., Heindl, W. A., Rothschild, R. E., Gruber, D. E., Kreykenbohm, I., Wilms, J., Kretschmar, P., Staubert, R. 2002, ApJ, 580, 394
 Collier Cameron A., Campbell C. G., 1993, A&A, 274, 309
 Chen K., Ruderman M., 1993, ApJ, 408, 179

Cui W., Morgan E. H., Titarchuk L. G., 1998, ApJ, 504, L27
 Donati J.-F., Collier Cameron A., 1997, MNRAS, 291,1
 Donati J.-F., Collier Cameron A., Hussain G.A.J., Semel M., 1999, MNRAS, 302, 437
 Donati, J.-F.; Jardine, M. M.; Gregory, S. G.; Petit, P.; Bouvier, J.; Dougados, C.; Mnard, F.; Collier Cameron, A.; Harries, T. J.; Jeffers, S. V.; Paletou, F., 2007, MNRAS, 380, 1297
 Donati J.-F., Jardine M. M., Gregory S. G. et al., 2008, MNRAS, 386, 1234
 Donati, J.-F., Skelly, M. B., Bouvier, J., Jardine, M. M., Gregory, S. G., Morin, J., Hussain, G. A. J., Dougados, C., Mnard, F., Unruh, Y., 2010, MNRAS, 402, 1426
 Donati, J.-F., Bouvier, J., Walter, F. M., Gregory, S. G., Skelly, M. B., Hussain, G. A. J., Flaccomio, E., Argiroffi, C., Grankin, K. N.; Jardine, M. M., et al. 2011, MNRAS, 412, 2454
 Elsner R. F., Lamb F. K., 1976, Nature, 262, 356
 Elsner R. F., Lamb F. K., 1977, ApJ, 215, 897
 Euchner F., Jordan S., Beuermann K., Gänsicke B. T., Hessman F. V., 2002, A&A, 390, 633
 Euchner F., Reinsch K., Jordan S., Beuermann K., Gänsicke B. T., 2005, A&A, 442, 651
 Euchner F., Jordan S., Beuermann K., Reinsch K., Gänsicke B. T., 2006, A&A, 451, 671
 Ghosh P., 2007, Rotation and Accretion Powered Pulsars: World Scientific Series in Astronomy and Astrophysics, Vol. 10., World Scientific Publishing Co., Pte. Ltd., Singapore.
 Ghosh P., Lamb F. K., 1978, ApJ, 223, L83
 Ghosh P., Lamb F. K., 1979, ApJ, 232, 259
 Ghosh P., Pethick C. J. Lamb F. K., 1977, ApJ, 578
 Gierliński M., Poutanen J., 2005, MNRAS, 359, 1261
 Grankin K. N., Melnikov S. Y., Bouvier J., Herbst W., Shevchenko V. S., 2007, A&A, 461, 18
 Gregory S. G., Jardine M., Simpson I. Donati J.-F., 2006, MNRAS, 371, 999
 Gregory S. G., Matt S. P., Donati J.-F., Jardine M., 2008, MNRAS, 1839, 1350
 Gregory, S.G., Jardine, M., Gray, C.G., & Donati, J.-F., 2010, Rep. Prog. Phys., 73, 126901
 Hartman J.M., Patruno A., Chakrabarty D., Kaplan D. L., Markwardt C. B., Morgan E. H., Ray P. S., van der Klis M., Wijnands R., 2008, ApJ, 675, 1468
 Hartman J.M., Patruno A., Chakrabarty D., Markwardt C. B., Morgan E. H., van der Klis M., Wijnands R., 2009, ApJ, 702, 1673
 Herbst W., Herbst D. K., Grossman E. J., 1994, AJ, 108, 1906
 Hussain G. A. J., Collier Cameron A., Jardine M. M. et al., 2009, MNRAS, 398, 189
 Ibragimov, A., & Poutanen, J., 2009, MNRAS, 400, 492
 Jardine M., Wood K., Collier Cameron A., Donati J.-F., Mackay D.H., 2002, MNRAS, 336, 1364
 Johns-Krull C., Valenti J.A., Koresko, C., 1999, ApJ, 516, 900
 Johns-Krull C. M., 2007, ApJ, 664, 975
 Kulkarni A. K., Romanova M. M., 2005, ApJ, 633, 349
 Kulkarni, A. K., Romanova, M. M. 2008, MNRAS, 386, 673
 Lamb F. K., Pethick C. J., Pines D., 1973, ApJ, 184, 271
 Lamb F. K., Boutloukos S., Van Wassenhove S., Chamberlain R. T., Lo K. H., Clare A., Yu W., Miller M.C., 2009a, ApJ, 706 417
 Lamb F. K., Boutloukos S., Van Wassenhove S., Chamberlain R. T., Lo K. H., Miller M. C., 2009b, ApJ, 705, L36
 Long M., Romanova M. M., Lovelace R. V. E., 2005, ApJ, 634, 1214
 ——— 2007, MNRAS, 374, 436
 ——— 2008, MNRAS, 386, 1274
 Long M., Romanova M. M., Lamb F., Kulkarni A.K., Donati J.-F., 2011, MNRAS, 413, 1061
 Lovelace, R.V.E., Romanova M. M., Bisnovatyi-Kogan, G.S. 2005, ApJ, 625, 957

Makishima, K., Mihara, T., Nagase, F., Tanaka, Y., *ApJ*, 525, 978.
 Matt S., Pudritz R. E., 2005, *MNRAS*, 356, 167
 Markwardt C. B., 2004, in *X-ray Timing 2003: Rossi and Beyond*,
 eds. P. Kaaret, F. K. Lamb, J. H. Swank, AIP Conf. Proc. 714, 217
 Meggitt S. M. A., Wickramasinghe D. T., 1989, *MNRAS*, 236, 31
 Mohanty S., Shu F. H., 2008, *ApJ*, 687, 1323
 Morgan E. H., Chakrabarty D., Wijnands R., van der Klis M., Mark-
 wardt C., 2003, in *Bulletin of the American Astronomical Society*,
 Vol. 35, 629
 Nishimura O., 2005, *PASJ*, 57, 769
 Payne, D. J. B., Melatos, A., 2004, *MNRAS*, 351, 569
 Payne, D. J. B., Melatos, A., 2006, *ApJ*, 652, 597
 Patruno A., Altamirano D., Hessels J.W.T., Casella P., Wijnands R.,
 van der Klis M., 2009a, *ApJ*, 690, 1856
 Patruno A., Wijnands R., & van der Klis M., 2009b, *ApJ*, 698, L60
 Patruno, A., Hartman, J. M., Wijnands, R., Chakrabarty, D., van der
 Klis, M., 2010, *ApJ*, 717, 1253
 Piroola V., Coyne G. V., Reiz A., 1987, *A&A*, 186, 120
 Percy J. R., Gryc W. K., Wong J. C.-Y., 2006, *PASP*, 118, 1390
 Poutanen, J., Ibragimov, A., Annala, M., 2009, *ApJ*, 706, L129
 Poutanen J., Gierliński M., 2003, *MNRAS*, 343, 1301
 Psaltis D., Chakrabarty D., 1999, *ApJ*, 521, 332
 Putman W. M., Lin S. -J., 2007, *J. Comp. Phys.*, 227, 55
 Romanova M. M., Long M., Lamb F., Kulkarni A.K., Donati J.-F.,
 2011a, *MNRAS*, 411, 915
 Romanova M. M., Ustyugova G. V., Koldoba A. V., Lovelace R. V.
 E., 2004, *ApJ*, 610, 920
 Romanova M. M., Ustyugova G. V., Koldoba A. V., Wick J.V.,
 Lovelace R. V. E., 2003, *ApJ*, 595, 1009
 Romanova M. M., Kulkarni A. K., Lovelace R. V. E., 2008, *ApJ*, 673,
 L171
 Romanova M. M., Ustyugova G. V., Koldoba A. V., Lovelace R. V.
 E., 2009, *MNRAS*, 399, 1802
 Romanova M. M., Ustyugova G. V., Koldoba A. V., Lovelace R. V.
 E., 2011b, *MNRAS*, in press (arXiv:1102.1089)
 Ruderman M. 1991, *ApJ*, 366, 261
 Ruderman M. 2005, *The Electromagnetic Spectrum of Neutron Stars*,
 Ed. by A. Baykal, S. K. Yerli, S. C. Inam, and S. Grebenev. NATO
 science series II: Mathematics, physics and chemistry, vol. 210,
 p.47. Springer, Dordrecht.
 Smirnov D. A., Lamzin S. A., Fabrika S. N., Chuntunov G. A., 2004,
Astron. Lett., 30, 456
 Thompson C., Duncan R.C., 1993, *ApJ*, 408, 194
 van der Klis M., 2000, *ASA&A*, 38, 717
 Warner B., 1995, *Cataclysmic Variable Stars*, Cambridge Univ. Press,
 Cambridge
 Wickramasinghe D. T., Ferrario, L., 2000, *PASP*, 112, 873
 Wijnands, R., & van der Klis, M. 1998, *Nature*, 394, 344